Cell Metabolism, Volume *17*

Supplemental Information

In Vivo HIF-Mediated Reductive Carboxylation Is Regulated by Citrate Levels and Sensitizes *VHL*-Deficient Cells to Glutamine Deprivation

Paulo A. Gameiro, Juanjuan Yang, Ana M. Metelo, Rocio Pérez-Carro, Rania Baker, Zongwei Wang, Alexandra Arreola, W. Kimryn Rathmell, Aria Olumi, Pilar López-Larrubia, Gregory Stephanopoulos, and Othon Iliopoulos

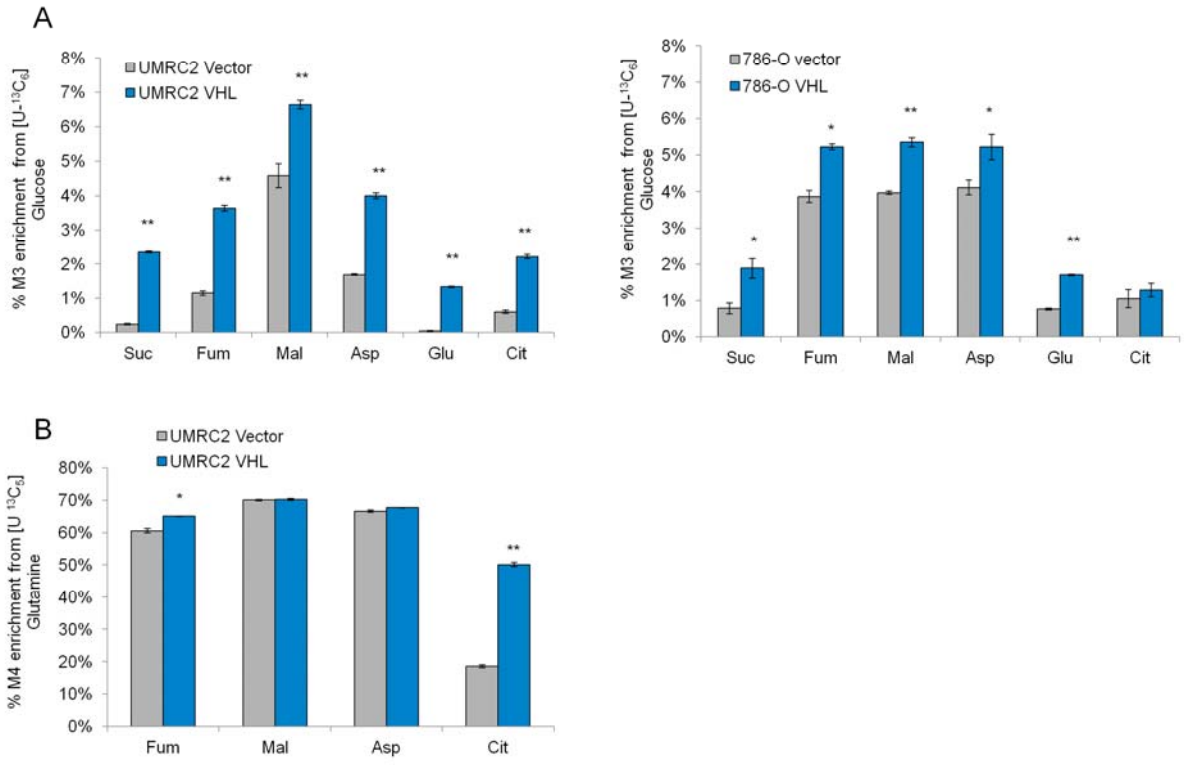

Figure S1. Evidence for Regulation of Glucose and Glutamine Utilization by pVHL in RCC Cells, Related to Figure 1

(A) Contribution of pyruvate carboxylation and *(B)* glutamine oxidation to the TCA cycle in RCC cells. Student's *t*-test compared *VHL*-reconstituted to vector-only RCC cells.

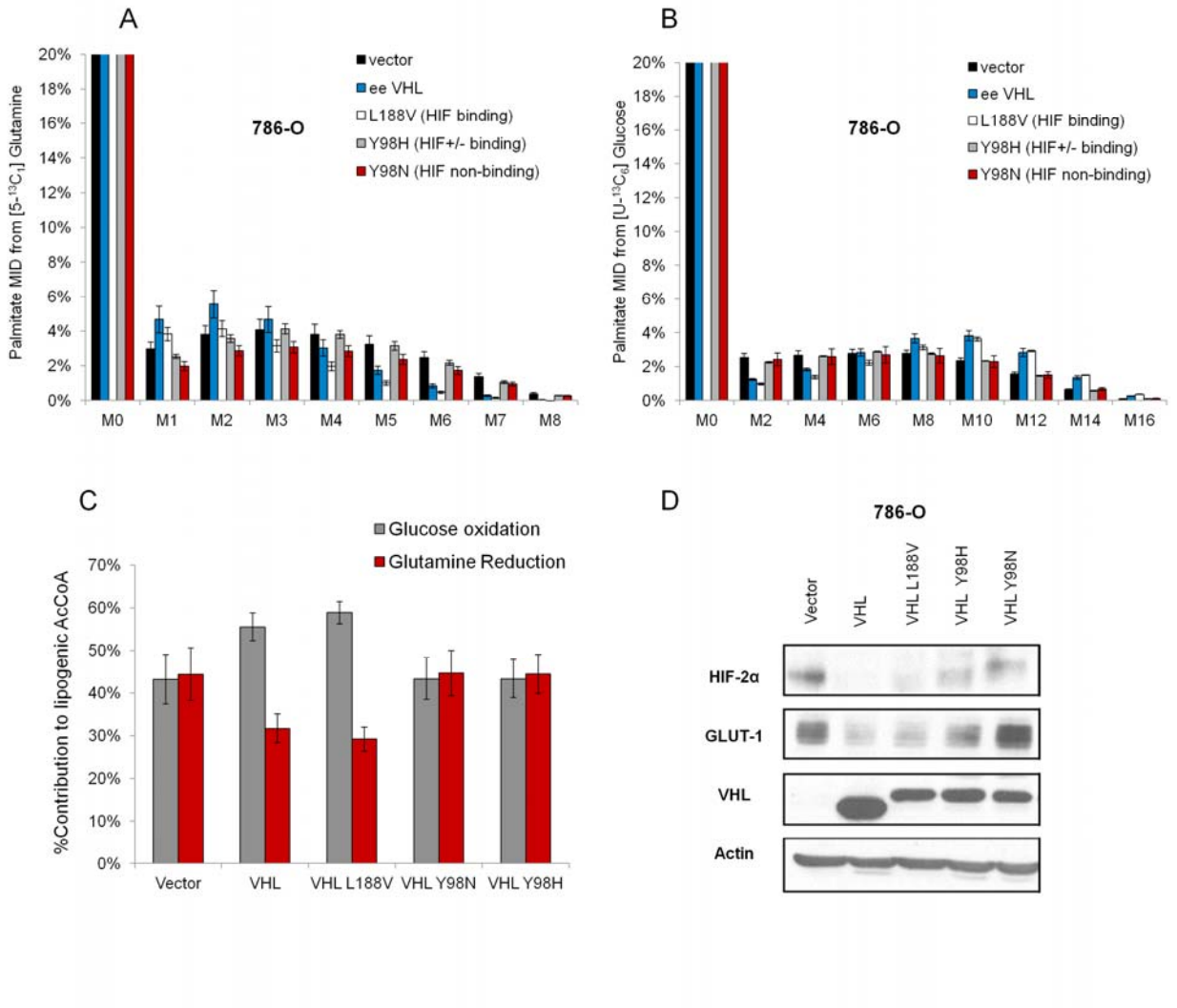

Figure S2. Regulation of Reductive Lipogenesis by the VHL-HIF Interaction in 786-O Cells, Related to Figure 2

The panel of mutant 786-O cells was cultured for 2-3 days with [5-$^{13}C_1$] glutamine or [U-$^{13}C_6$] glucose. *(A-B)* Mass isotopomer distributions (MIDs) of palmitate in 786-O cells labeled with [5-$^{13}C_1$] glutamine *(A)* or [U-$^{13}C_6$] glucose *(B)*. *(C)* Specific contribution from glucose oxidation and glutamine reduction to lipogenic acetyl-CoA in a panel of 786-O-derived cell lines, using the ISA method *(D)* HIF-2α, VHL and GLUT1 protein levels in vector-only, VHL-reconstituted and VHL mutant 786-O cells.

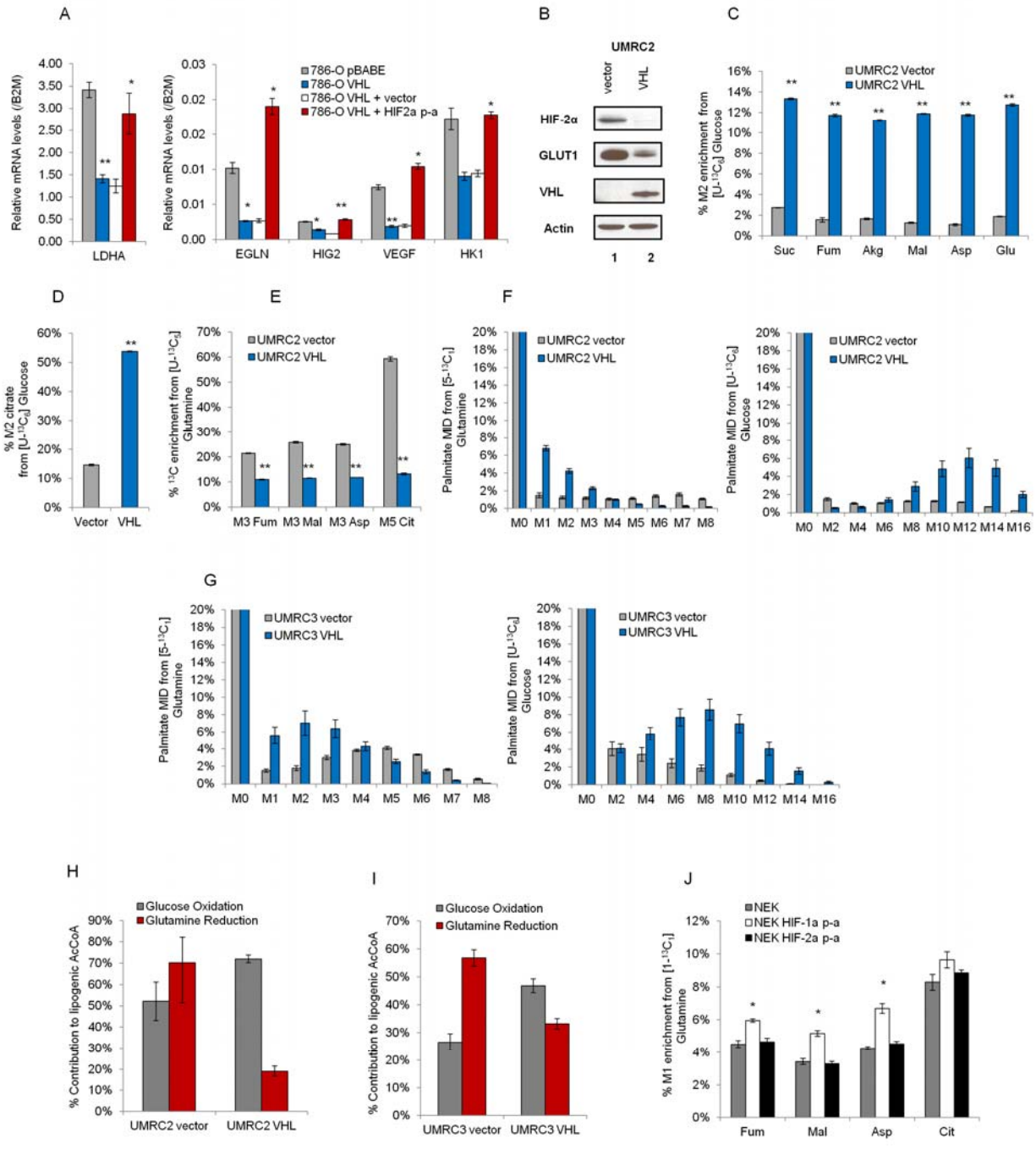
A
Relative mRNA levels (/B2M)
LDHA
EGLN
HIG2
VEGF
HK1
786-O pBABE
786-O VHL
786-O VHL + vector
786-O VHL + HIF2a p-a
B
UMRC2
vector
VHL
HIF-2α
GLUT1
VHL
Actin
1
2
C
% M2 enrichment from [U-13C6] Glucose
UMRC2 Vector
UMRC2 VHL
Suc
Fum
Akg
Mal
Asp
Glu
D
% M2 citrate from [U-13C6] Glucose
Vector
VHL
E
% 13C enrichment from [U-13C5] Glutamine
UMRC2 vector
UMRC2 VHL
M3 Fum
M3 Mal
M3 Asp
M5 Cit
F
Palmitate MID from [5-13C1] Glutamine
Palmitate MID from [U-13C6] Glucose
UMRC2 vector
UMRC2 VHL
M0 M1 M2 M3 M4 M5 M6 M7 M8
M0 M2 M4 M6 M8 M10 M12 M14 M16
G
Palmitate MID from [5-13C1] Glutamine
Palmitate MID from [U-13C6] Glucose
UMRC3 vector
UMRC3 VHL
M0 M1 M2 M3 M4 M5 M6 M7 M8
M0 M2 M4 M6 M8 M10 M12 M14 M16
H
% Contribution to lipogenic AcCoA
Glucose Oxidation
Glutamine Reduction
UMRC2 vector
UMRC2 VHL
I
% Contribution to lipogenic AcCoA
Glucose Oxidation
Glutamine Reduction
UMRC3 vector
UMRC3 VHL
J
% M1 enrichment from [1-13C1] Glutamine
NEK
NEK HIF-1a p-a
NEK HIF-2a p-a
Fum
Mal
Asp
Cit

Figure S3. Evidence for Regulation of Reductive Carboxylation by pVHL and HIF-2α P-A Mutant in RCC Cells, Related to Figure 3

(A) mRNA expression level of HIF-2α target genes, normalized that of the beta2-microglobulin. *(B)* HIF-2α, pVHL and GLUT1 protein levels in *VHL*-deficient/*VHL*-reconstituted UMRC2 cells. *(C-E)* Regulation of glucose oxidation *(C, D)* and reductive carboxylation *(E)* by reintroduction of pVHL in *VHL*-deficient UMRC2 cells. *(F-G)* Mass isotopomer distributions (MIDs) of palmitate in UMRC2 *(F)* and UMRC3 cells *(G)* labeled with [5-$^{13}C_1$] glutamine or [U-$^{13}C_6$] glucose. *(H-I)* Specific contribution from glucose oxidation and glutamine reduction to lipogenic acetyl-CoA in UMRC2 *(H)* and UMRC3 *(I)* cells. (J) Regulation of reductive carboxylation in neonatal epithelial kidney cells (NEK) by mouse HIF1a p-a and HIF2a p-a paralogues, induced for 72 hours. Student's *t*-test compared wild type EE-VHL, mutant HIF2α p-a, or inducible HIF-1α/2α expressing cells to corresponding control cells.

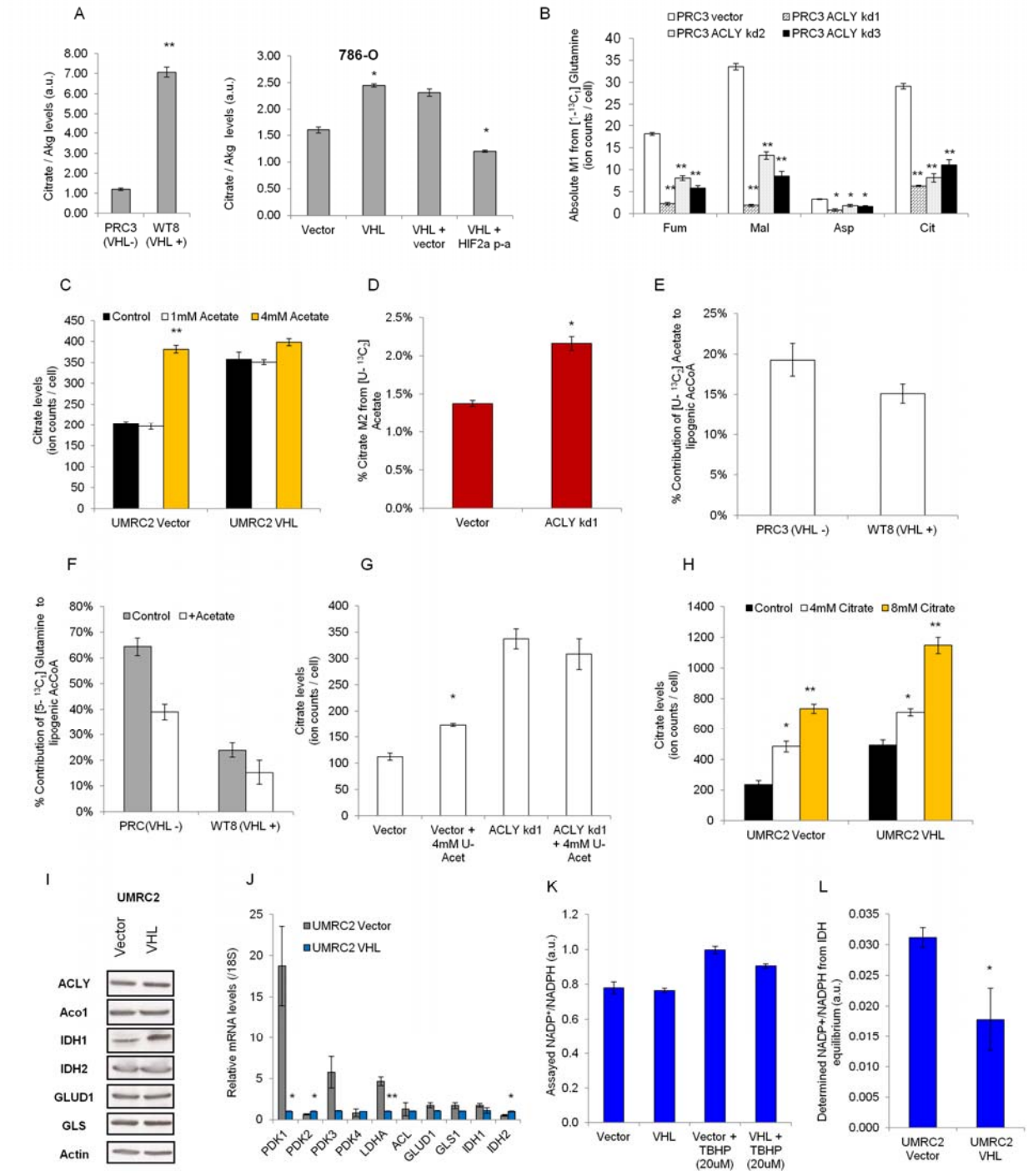
A
Citrate / Akg levels (a.u.)
PRC3 (VHL-)
WT8 (VHL +)
786-O
Vector
VHL
VHL + vector
VHL + HIF2a p-a
B
PRC3 vector
PRC3 ACLY kd1
PRC3 ACLY kd2
PRC3 ACLY kd3
Absolute M1 from [1-13C2] Glutamine (ion counts / cell)
Fum
Mal
Asp
Cit
C
Control
1mM Acetate
4mM Acetate
Citrate levels (ion counts / cell)
UMRC2 Vector
UMRC2 VHL
D
% Citrate M2 from [U-13C2] Acetate
Vector
ACLY kd1
E
% Contribution of [U-13C2] Acetate to lipogenic AcCoA
PRC3 (VHL -)
WT8 (VHL +)
F
Control
+Acetate
% Contribution of [5-13C1] Glutamine to lipogenic AcCoA
PRC(VHL -)
WT8 (VHL +)
G
Citrate levels (ion counts / cell)
Vector
Vector + 4mM U-Acet
ACLY kd1
ACLY kd1 + 4mM U-Acet
H
Control
4mM Citrate
8mM Citrate
Citrate levels (ion counts / cell)
UMRC2 Vector
UMRC2 VHL
I
UMRC2
Vector
VHL
ACLY
Aco1
IDH1
IDH2
GLUD1
GLS
Actin
J
UMRC2 Vector
UMRC2 VHL
Relative mRNA levels (/18S)
PDK1
PDK2
PDK3
PDK4
LDHA
ACL
GLUD1
GLS1
IDH1
IDH2
K
Assayed NADP+/NADPH (a.u.)
Vector
VHL
Vector + TBHP (20uM)
VHL + TBHP (20uM)
L
Determined NADP+/NADPH from IDH equilibrium (a.u.)
UMRC2 Vector
UMRC2 VHL

Figure S4. Evidence for Induction of Reductive Carboxylation by Mass Action in HIF-Expressing Cells, Related to Figure 5

(A) Citrate to α-ketoglutarate ratio observed in PRC3/WT8 cells and in the panel of 786-O cell lines used in our isotopic studies. *(B) Total* contribution of reductive carboxylation in vector control/ACLY knocked-down PRC3 cells, determined by the total M1 counts of TCA cycle metabolites. *(C)* Rescue of citrate levels by acetate addition in the panel of UMRC2 cells. *(D)* Contribution of [U-$^{13}C_2$] acetate to citrate production in vector control/ACLY knocked-down PRC3 cells. *(E)* Specific contribution of [U-$^{13}C_2$] acetate to lipid carbon and *(F)* the affect of naturally labeled acetate on the contribution of glutamine reduction to lipogenesis in PRC3/WT8 cells. *(G)* Rescue of intracellular citrate levels by acetate addition in control/ACLY knocked-down PRC3 cells. *(H)* Rescue of intracellular citrate levels by exogenous citrate in the panel of UMRC2 cells. *(I)* Immunoblot for glutaminase (GLS), glutamate dehydrogenase 1 (GLUD1), isocitrate dehydrogenase 2 (IDH2), isocitrate dehydrogenase 1 (IDH1), aconitase/IRP1 (Aco1), and ATP-citrate lyase (ACLY) in UMRC2 cells reconstituted with empty vector control (lane 1) or wild type EE-VHL (lane 2). *(J)* mRNA levels of pyruvate dehydrogeanse kinase 1 (PDK1), PDK2, PDK3, PDK4 and glutamine-metabolizing enzymes in the panel of UMRC2 cells. *(K-L)* $NADP^+$/NADPH ratios in VHL-deficient/VHL-reconstituted UMRC2 cells assayed in the cell extract *(I)* and determined using the ratios of the oxidized and reduced metabolites of the NADPH-linked IDH equilibrium *(J)*. *tert*-Butyl hydroperoxide (TBHP) was used as an oxidant control. Student's *t*-test compare: 1) *VHL*-reconstituted or mutant HIF p-a to corresponding control cells (for panels A, J and L), 2) ACLY knocked-down to control PRC3 cells (for panels B and D), and 3) acetate or citrate-rescued cells to correspondent controls (for panels C, G and H).

Table S1. Determined Fluxes and their 95% Confidence Intervals for PRC3/WT8 Cells Estimated from MFA Model Using [U-$^{13}C_6$] Glucose and [1-$^{13}C_1$] Glutamine Tracer Data Sets

Reaction	PRC3 (VHL-)			WT8 (VHL+)		
	Flux pmol/cell/hour	95% Confidence Intervals		Flux pmol/cell/hour	95% Confidence Intervals	
		Lower	Upper		Lower	Upper
Glycolysis	0.79	0.78	0.81	0.72	0.71	0.73
Glc.x → G6P	0.79	0.43	0.81	-0.59	-0.67	0.33
G6P → F6P	0.00	0.00	Inf	0.04	0.00	Inf
G6P ↔ F6P	0.79	0.67	0.81	0.28	0.26	0.32
F6P→DHAP + GAP	0.79	0.67	0.81	0.28	0.26	0.32
DHAP→ GAP	0.47	0.00	Inf	0.00	0.00	Inf
DHAP ↔ GAP	1.58	1.46	1.62	1.01	0.98	1.02
GAP→3PG	0.00	0.00	Inf	0.37	0.00	Inf
GAP ↔ 3PG	1.58	1.46	1.62	1.01	0.98	1.02
3PG → Pyr.c	1.37	1.33	1.41	0.95	0.93	0.97
Pyr.c ↔ Lac	0.87	0.00	Inf	0.21	0.00	Inf
Lac → Lac.x	1.37	1.33	1.41	0.95	0.93	0.97
Pentose Phosphate Pathway						
G6P → P5P + CO2	0.00	0.00	0.36	1.31	0.39	1.40
P5P + P5P → S7P + GAP	0.00	0.00	0.12	0.44	0.13	0.47
P5P + P5P ↔ S7P + GAP	2.55	0.00	Inf	1.10E+04	0.00E+00	Inf
S7P + GAP → F6P + E4P	0.00	0.00	0.12	0.44	0.13	0.47
S7P + GAP ↔ F6P + E4P	0.28	0.00	Inf	0.70	0.00	Inf
P5P + E4P → F6P + GAP	0.00	0.00	0.12	0.44	0.13	0.47
P5P + E4P ↔ F6P + GAP	1.97	0.00	Inf	2.28	0.00	Inf
Anaplerotic reactions						
Pyr.m + CO2 → Oac	0.02	0.00	0.16	0.00	0.00	0.02
Mal → Pyr.m + CO2	0.16	0.13	0.32	0.12	0.12	0.12
Mal ↔ Pyr.m + CO2	0.05	0.00	0.16	0.01	0.01	0.02
Glu → Akg	0.14	0.13	0.16	0.12	0.12	0.12
Glu ↔ Akg	10.62	0.63	Inf	1.43E+05	3.07E+00	Inf
Oac → Asp	0.00	0.00	0.00	0.00	0.00	0.00
Oac ↔ Asp	0.32	0.00	Inf	0.47	0.00	Inf
TCA cycle						
Pyr.m →AcCoA.m + CO2	0.03	0.02	0.05	0.17	0.15	0.19
AcCoA.m + Oac → Cit	0.03	0.02	0.05	0.17	0.15	0.19
Cit →Akg + CO2	-0.02	-0.03	-0.01	0.01	0.01	0.01
Cit ↔ Akg + CO2	0.07	0.04	0.15	0.02	0.02	0.03
Akg → Suc + CO2	0.12	0.11	0.13	0.13	0.12	0.13
Suc → Fum	0.12	0.11	0.13	0.13	0.12	0.13
Suc ↔ Fum	0.01	0.00	0.03	0.00	0.00	0.03
Fum → Mal	0.12	0.11	0.13	0.13	0.12	0.13
Fum ↔ Mal	2.08	0.68	Inf	1.07	0.38	Inf
Mal → Oac	-0.04	-0.20	-0.01	0.01	0.01	0.01
Mal ↔ Oac	1.63E+02	9.54E-	Inf	2.21E+04	8.77E-01	Inf
Cit → AcCoA.c + Oac	0.05	0.03	0.08	0.17	0.14	0.19
AcCoA.c → Palm	0.05	0.03	0.08	0.17	0.14	0.19
Glutamine metabolism						
Pyr.c → Ala	0.00	0.00	0.00	0.00	0.00	0.00
Pyr.c ↔ Ala	4.23	0.00	Inf	0.96	0.00	Inf
Gln.x → Gln	0.19	0.18	0.21	0.14	0.14	0.14
Gln → Glu	0.19	0.18	0.21	0.14	0.14	0.14
Glu →Glu.x	0.05	0.05	0.06	0.02	0.02	0.02
Mixing/Dilution						
Pyr.c → Pyr.m	-0.11	-0.13	-0.11	0.05	0.03	0.07
Pyr.c ↔ Pyr.m	0.04	0.02	0.06	0.22	0.20	0.33
Pyr.c → Pyr.mnt	0.33	0.19	0.38	0.00	0.00	0.35
Pyr.m → Pyr.mnt	0.00	0.00	0.00	0.00	0.00	0.00

Supplemental Experimental Procedures

Cell Culture and Metabolic Labeling

PRC3 and WT8 were described before (Iliopoulos et al., 1995). For the metabolic labeling experiments, cells were cultured in 4mM glutamine (Gln) tracer and 25mM unlabeled glucose (Glu) or 25mM [U-$^{13}C_6$] Glu and 4mM unlabeled Gln (Cambridge Isotope Labs). Metabolite steady-state labeling corresponded to 24hour of labeling. For cell viability assays, cells were cultured in basal DMEM supplemented with 25mM glucose, 1mM glutamine and 10% dialyzed FBS. Cell number was determined manually and viability determined by trypan blue exclusion. Neonatal epithelial kidney (NEK) cells were derived from transgenic mice engineered to harbor UBCcreER; Rosa 26 lox-stop-lox HIF1dPA or UBCcreER; Rosa 26 lox-stop-lox HIF2dPA or UBCcreER as control. NEK cell were cultured in DMEM/F12 medium supplemented with insulin-transferrin-selenium (Invitrogen 41400-045) and EGF (Gemini Bio300-110).

Metabolic Flux Analysis and Isotopomer Spectral Analysis

Mass isotopomer distributions (MIDs) for each metabolite are simulated using initial "guess" flux vectors, the substrate labeling information and a stoichiometric matrix outlined by the reaction network and atom transitions. The simulated MIDs are compared with measured MIDs and the flux vector is iteratively adjusted by minimizing the residuals between simulated and measured MIDs, as previously described (Antoniewicz et al., 2007; Metallo et al., 2012). 95% confidence intervals were determined as described before (Antoniewicz et al., 2006) . Likewise, ISA was performed to estimate the tracer enrichment in the acetyl-CoA pool and the percentage of newly synthesized palmitate (Yoo et al., 2004) . MIDs were corrected for natural isotopic abundance.

Metabolite Analysis of Extracellular Medium

Cells were seeded at low density in basal DMEM, the spent medium collected at the end of a 72 hours growth period and analyzed using a Yellow Springs Instruments (YSI) 7100. The specific growth rate (μ) was estimated through regression of equation 1. Specific rates were calculated using the normalized consumption/secretion coefficient (Δn/ΔX) which is multiplied by the estimated specific growth rate (μ), according to equation 2, in which Δn is the measured difference of moles consumed/produced, ΔX is the difference in cell density (cells/cm^2), and ν is the specific uptake/secretion flux.

$$Ln\,(X) = Ln\,(X_o) + \mu t \qquad (1)$$

$$\nu = \mu \frac{\Delta n}{\Delta X} \qquad (2)$$

Determination of NADP$^+$/NADPH Ratios

NAD(P)$^+$/NAD(P)H ratios were also determined employing the method developed in Krebs lab, as described therein (Veech et al., 1969). In brief, the isocitrate dehydrogenase equilibrium system (equation 3) was used to determine the ratio of NADP$^+$/NADPH. Cells were rinsed twice with 2ml PBS before extraction to eliminate the contribution of extracellular metabolites. Ratios were obtained from individualized metabolite measurements in the same GC-MS injection.

$$\frac{[\alpha - ketoglutarate]\,[CO2]\,[NADPH]}{[isocitrate][NADP+]} = K\,(GDH) = 1.17\ \mathrm{M} \qquad (3)$$

Plasmids and Western Blots

pBABEpuro plasmids expressing HA-VHL mutants Y98H, Y98N, Y112H, Y112N, L188V and pBABEhygro plasmid expressing HA-HIF2a p-a were purchased from Addgene**.** EE-VHL were constructed by PCR amplification of wild type VHL with oligos forward 5'- GCGCGGATCCG CCACCATGGAATACATGCCCATGGAA ATGCCCCGGAGGGCGGAG-3' and reverse 5'-GCGCGAATTCAATCTCCCATCCGTTGATGTGCAATG-3'. PCR product was restricted with BamHI and EcoRI and ligated into pBABE puro vector. Plasmids encoding shRNA targeting PDK1 (CCAGGGTGTGATTGAATACAA and GATCAGTGAATGCTTGTGAAA), ACLY (CGAGGACTTGTACTTCACCTA, GCCTCAAGATACTATACATTT and GCCTAAGTACT CTTGCCAGTT) and luciferase as control were obtained from the Broad TRC library available at MGH. Targeting sequences Proteins were extracted and immunobloted as described before (Zimmer et al., 2008), using antibodies recognizing the following proteins: HIF2a (Novus NB100-122), HIF1a (BD Biosciences 610958), VHL (IG32), GLUT1 (Alpha Diagnostics), GLS (Abnova), GLUD1 and IDH2 (Novus Biologicals), IDH1 (Cell Signaling), ACLY (Cell Signaling), PDK.1 (Cell Signaling) and Actin (Neomarkers).

Animal Studies

For *in vivo* labeling studies, UMRC3 cells were injected in both flanks of nu/nu mice. ^{13}C labeling infusions were begun when tumors reached an external diameter of 1-1.5 cm. Animals (n=3) were infused with [1-$^{13}C_1$] glutamine, as previously described (Marin-Valencia et al., 2012). In brief, a bolus of 0.28 mg/g bodyweight (300 μl) was administrated over 1 min and followed by a continuous infusion of 0.005mg/g/min at 450 μl/h during 0.5, 1, 2 or 6 hours. Non-infused animals were used as controls for further analysis. At the end of indicated infusion times,

blood was collected from the heart and animals sacrificed by cervical dislocation. Tumors and kidneys were quickly dissected, weighted, frozen in liquid nitrogen and stored at -80 ^{o}C. Tumors weighted between 1.124 ± 0.136 g (mean ± SEM). Tumors from one flank were used for NMR analysis and extracted as previously described (Cerdan et al., 1990). Tumors and kidneys from the other flank were used for GC-MS analysis and metabolites extracted as previously described (Wu et al., 2008).

^{13}C NMR Spectroscopy

High-resolution proton-decoupled ^{13}C NMR spectra of tumor extracts were obtained at 11.7 T (125.13 Hz, 25 ^{o}C, pH = 7.2) in a Bruker AVANCE 500WB NMR spectrometer using a commercial (5 mm) triple-resonance probe (^{1}H, ^{13}C, ^{2}H) optimized for direct ^{13}C detection. The acquisition conditions were: 30^{o} flip angle, 30 kHz spectral width, 3 s relaxation delay, and 1.09 s acquisition time. Proton decoupling was gated during all acquisition using a broad-band composite pulse decoupling sequence, and chemical shifts were calibrated with dioxane (0.1 % vol/vol, 67.4 ppm). Resonance assignments were based on literature values and internal standards. Spectra deconvolution was performed using the software MestRec-C 4.8.6.0. (Mestrelab Research S.L.). ^{13}C NMR resonance areas were normalized relative to the dioxane resonance area used as internal reference.

Supplemental References

Antoniewicz, M.R., Kelleher, J.K., and Stephanopoulos, G. (2006). Determination of confidence intervals of metabolic fluxes estimated from stable isotope measurements. Metabolic Engineering *8*, 324-337.

Antoniewicz, M.R., Kelleher, J.K., and Stephanopoulos, G. (2007). Elementary metabolite units (EMU) - A novel framework for modeling isotopic distributions. Metabolic Engineering *9*, 68-86.

Cerdan, S., Kunnecke, B., and Seelig, J. (1990). Cerebral metabolism of [1,2-13C2]acetate as detected by in vivo and in vitro 13C NMR. J Biol Chem *265*, 12916-12926.

Iliopoulos, O., Kibel, A., Gray, S., and Kaelin, W.G., Jr. (1995). Tumour suppression by the human von Hippel-Lindau gene product. Nat Med *1*, 822-826.

Marin-Valencia, I., Yang, C., Mashimo, T., Cho, S., Baek, H., Yang, X.L., Rajagopalan, K.N., Maddie, M., Vemireddy, V., Zhao, Z., *et al.* (2012). Analysis of tumor metabolism reveals mitochondrial glucose oxidation in genetically diverse human glioblastomas in the mouse brain in vivo. Cell Metab *15*, 827-837.

Metallo, C.M., Gameiro, P.A., Bell, E.L., Mattaini, K.R., Yang, J., Hiller, K., Jewell, C.M., Johnson, Z.R., Irvine, D.J., Guarente, L., *et al.* (2012). Reductive glutamine metabolism by IDH1 mediates lipogenesis under hypoxia. Nature *481*, 380-384.

Veech, R.L., Eggleston, L.V., and Krebs, H.A. (1969). The redox state of free nicotinamide-adenine dinucleotide phosphate in the cytoplasm of rat liver. Biochem J *115*, 609-619.

Wu, H., Southam, A.D., Hines, A., and Viant, M.R. (2008). High-throughput tissue extraction protocol for NMR- and MS-based metabolomics. Analytical Biochemistry *372*, 204-212.

Yoo, H., Stephanopoulos, G., and Kelleher, J.K. (2004). Quantifying carbon sources for de novo lipogenesis in wild-type and IRS-1 knockout brown adipocytes. Journal of Lipid Research *45*, 1324-1332.

Zimmer, M., Ebert, B.L., Neil, C., Brenner, K., Papaioannou, I., Melas, A., Tolliday, N., Lamb, J., Pantopoulos, K., Golub, T., *et al.* (2008). Small-Molecule Inhibitors of HIF-2a Translation Link Its 5'UTR Iron-Responsive Element to Oxygen Sensing. Molecular Cell *32*, 838-848.